VII International Conference on Computational Methods in Marine Engineering
MARINE 2017
M. Visonneau, P. Queutey and D. Le Touzé (Eds)

MULTI-OBJECTIVE HULL-FORM OPTIMIZATION OF A SWATH CONFIGURATION VIA DESIGN-SPACE DIMENSIONALITY REDUCTION, MULTI-FIDELITY METAMODELS, AND SWARM INTELLIGENCE

RICCARDO PELLEGRINI[⋆], ANDREA SERANI[⋆], STEFAN HARRIES[†] AND MATTEO DIEZ[⋆]

[⋆]CNR-INSEAN, National Research Council-Marine Technology Research Institute, Rome, Italy
e-mail: matteo.diez@cnr.it

[†]Friendship Systems AG, Potsdam, Germany
e-mail: harries@friendship-systems.com

Key words: Simulation-based design, Hull-form optimization, Design-space dimensionality reduction, Karhunen-Loève expansion, Multi-fidelity metamodels, Multi-objective particle swarm optimization

Abstract. A multi-objective simulation-based design optimization (SBDO) is presented for the resistance reduction and displacement increase of a small water-plane area twin hull (SWATH). The geometry is realized as a parametric model with the CAESES® software, using 27 design parameters. Sobol sampling is used to realize design variations of the original geometry and provide data to the design-space dimensionality reduction method by Karhunen-Loève expansion. The hydrodynamic performance is evaluated with the potential flow code WARP, which is used to train a multi-fidelity metamodel through an adaptive sampling procedure based on prediction uncertainty. Two fidelity levels are used varying the computational grid. Finally, the SWATH is optimized by a multi-objective deterministic version of the particle swarm optimization algorithm. The current SBDO procedure allows for the reduction of the design parameters from 27 to 4, resolving more than the 95% of the original geometric variability. The metamodel is trained by 117 coarse-grid and 27 fine-grid simulations. Finally, significant improvements are identified by the multi-objective algorithm, for both the total resistance and the displacement.

1 INTRODUCTION

Simulation-based design optimization (SBDO) assists the designer in the design process of complex engineering systems (such as aerial, ground, or maritime vehicles). In shape optimization, SBDO combines shape modification methods, the assessment of the design performances, and single or multi-objective optimization algorithms.

The shape modification can be performed by applying modification operators to the original design or defining the geometry through a parametric model [1]. Each parameter may be consid-

ered as a design variable for the optimization process, therefore the number of design variables may easily be significantly large for complex models and geometries. Recent research has focused on research space variability and dimensionality reduction as an essential part of SBDO. A quantitative approach based on the Karhunen-Loève expansion (KLE) has been formulated for a pre-optimization assessment of the shape modification variability and the definition of a reduced-dimensionality global model of the shape design [2].

The SBDO process often requires computationally expensive physics-based solvers to achieve accurate solutions. In order to reduce the computational cost of the SBDO process, metamodels are often used. These have been successfully developed and applied in many engineering fields [3]. Volpi et al. [4] presented a dynamic radial basis functions (RBF) metamodel for ship hydrodynamics problems. Its extension to design optimization has been presented in [5]. Lately, Giselle et al. [6] presented a survey on parallel surrogate-assisted global optimization for expensive functions.

Combining metamodelling methods with multi-fidelity approximations potentially leads to a further reduction of the computational cost. Multi-fidelity approximation methods have been developed with the aim of combining to some extent the accuracy of high-fidelity solvers with the computational cost of low-fidelity solvers [7]. Correction methods, such as additive and/or multiplicative approaches, are used to build multi-fidelity metamodels. High- and low-fidelity models may be determined by the physical model [7], and/or the size of the computational grid [8]. Multi-fidelity metamodels have been used for engineering applications including ships [9, 10].

For engineering applications, global derivative-free optimization algorithms represent an advantageous option for their (often common) ease of implementation and capability of providing adequate solutions to the optimization problem. Among this kind of algorithms, particle swarm optimization (PSO) was originally introduced [11] as a global derivative-free metaheuristics for single-objective optimization. The algorithm makes use of cognitive and social attractors based on individual and population optima, in order to steer the swarm dynamics. PSO has been extended to multi-objective optimization (MOPSO) in [12]. Generally, MOPSO extends the concept of cognitive and social attractors to the multi-objective context, using individual and population Pareto fronts, sub-swarms, or aggregate objective functions. A comprehensive survey on MOPSO variants has been provided in [13]. Most PSO (both single- and multi-objective) formulations include stochastic methods and/or random coefficients. This implies that in order to assess the algorithm performance, statistically significant results need to be produced, through extensive numerical campaigns. Such an approach is often too expensive (from the computational viewpoint) and therefore not practicable in SBDO (especially when computationally expensive solvers are used directly). For this reason, efficient deterministic approaches, namely deterministic PSO (DPSO) [14] and multi-objective deterministic PSO (MODPSO) [15] have been developed and successfully applied in SBDO.

The objective of the present work is the application and preliminary assessment of a SBDO methodology, based on design space dimensionality reduction, adaptive multi-fidelity metamodel (AMFM), and multi-objective deterministic particle swarm optimization, to a 36.5 m small water-plane area twin hull (SWATH) configuration.

The parametric geometry of the SWATH is produced with the computer-aided design (CAD) environment integrated in CAESES®, developed by FRIENDSHIP SYSTEMS. Subsequently, the design-space dimensionality reduction of the parametric model is performed by KLE [2].

The hydrodynamic performance is assessed by the potential flow solver WARP, developed at CNR-INSEAN [16]. The evaluations provided by WARP are used to build the AMFM of the total resistance and the displacement with a coarse and a fine panel grid. Finally, the MODPSO formulation presented in [17] is used for the multi-objective optimization with the aim of reducing the resistance in calm water at 18 kn and increasing the displacement.

2 PROBLEM STATEMENT AND SBDO METHODS

2.1 Model geometry and optimization problem

The SWATH is designed as two torpedoes connected to the upper platform by a couple of twin symmetric narrow struts for each hull (for a total of four struts). The main geometric particulars are: overall length $L_{\mathrm{OA}} = 36.50$ m (without propeller/rudder); torpedo maximum diameter $D = 4.50$ m; inter-axis distance $D_{\mathrm{H}} = 20.00$ m; first strut leading edge position $L_1 = 6.00$ m, struts length $S_{\mathrm{L}} = 12.00$ m, and struts clearance $S_{\mathrm{C}} = 5.15$ m; drought $T = 6.31$ m; wet surface $S_{\mathrm{W}} = 1064$ m^2 and water-plane area $A_{\mathrm{WP}} = 38.88$ m^2; displacement $\nabla = 982.23$ m^3.

A multi-objective optimization for calm water performances at 18 kn is sought after, as a significant test case for the SBDO methodology. The optimization problem reads

$$\begin{aligned} &\text{minimize } \mathbf{f}(\mathbf{x}) = \{R_T(\mathbf{x}), -\nabla(\mathbf{x})\}^T, \text{ with } \mathbf{x} \in \mathcal{D} \subset \mathbb{R}^{N_{\mathrm{dv}}} \\ &\text{subject to } \mathbf{l} \leq \mathbf{x} \leq \mathbf{u} \end{aligned} \tag{1}$$

where $\mathbf{x}$ is the design variable vector, R_T is the total resistance, ∇ is the ship displacement, N_{dv} is the number of design variables, and finally $\mathbf{l}$ and $\mathbf{u}$ are the lower and upper bounds for $\mathbf{x}$.

The geometry is realized as a parametric model in CAESES®, using a set $\mathbf{x}$ of 27 parameters. These parameters define, among other design features, the overall length, the struts clearance, the curvature of the torpedo nose, and the torpedo diameter. The inter-axis distance is held constant. Figure 1 shows the complete SWATH model as produced by CAESES® (a) and a simplified version used for the numerical simulations (b).

Critical design requirements and constraints associated to the modification of the displacement, water-plane area, and geometry of the struts (such as intact pitch and roll stability, seakeeping, and structural analysis) are beyond the scope of the present demonstration and will be addressed in future research.

2.2 Production of design variants through the CAESES® system

CAESES® (CAE System Empowering Simulation) by FRIENDSHIP SYSTEMS AG provides simulation-ready parametric CAD for complex shapes. The embedded CAD environment provides, beside all the most used features for modelling, specific tools for the ship hull and blade (for both propellers and turbo-machinery) design. Other features are provided for helping the designer to assess the quality of the parametric model (such as parameter sensitivity analysis). Furthermore, design modifications are allowed both with pseudo-random variation of design parameters or the free-form deformation techniques.

In the present work, the Sobol engine available in CAESES® is used for producing pseudo-random variations of the 27 geometric parameters. The Sobol method [18] provides a uniform

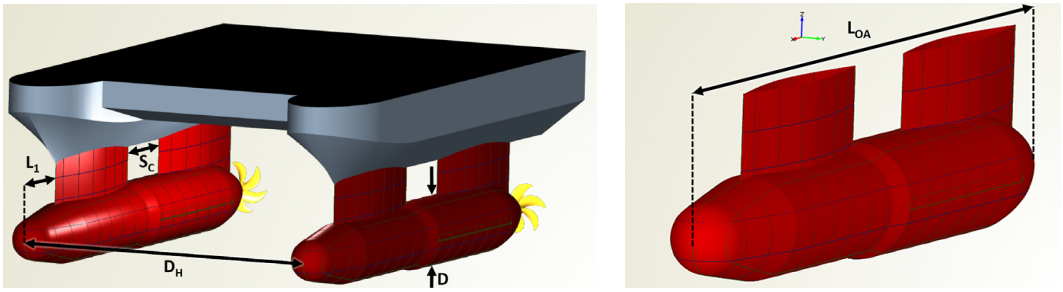

(a) CAESES® model

(b) Simplified model for numerical simulations

Figure 1: SWATH model

distribution of the parameters of the design space under investigation, which is used as the input of the design-space dimensionality reduction procedure.

2.3 Design-space dimensionality reduction by KLE

The Karhunen-Loève expansion of the shape modification vector produced by the Sobol method provides a pre-optimization (offline) assessment of the shape modification variability and the definition of a reduced-dimensionality global model of the shape modification vector [2]. Similar formulations have been developed and applied to elastic deformation of structures, including modal identification studies [19, 20].

A brief description of the method is recalled in the following. This can be applied with any shape modification method. Consider a geometric domain of interest $\mathcal{G}$, which identifies the initial shape, and a set of coordinates $\boldsymbol{\xi} \in \mathcal{G}$. Assume that the design variables $\mathbf{x}$ defines a shape modification vector $\boldsymbol{\delta}(\boldsymbol{\xi}, \mathbf{x})$. Consider the design variables $\mathbf{x}$ as belonging to a stochastic domain $\mathcal{D}$ with associated probability density function $p(\mathbf{x})$. The associated mean shape modification is evaluated as

$$\langle \boldsymbol{\delta} \rangle = \int_{\mathcal{D}} \boldsymbol{\delta}(\boldsymbol{\xi}, \mathbf{x}) p(\mathbf{x}) \mathrm{d}\mathbf{x} \tag{2}$$

If one defines the internal product in $\mathcal{G}$ as

$$(\mathbf{f}, \mathbf{g}) = \int_{\mathcal{G}} \mathbf{f}(\boldsymbol{\xi}) \cdot \mathbf{g}(\boldsymbol{\xi}) \, \mathrm{d}\boldsymbol{\xi} \tag{3}$$

with associated norm $\|\mathbf{f}\| = (\mathbf{f}, \mathbf{f})^{1/2}$, the variance associated to the shape modification vector (geometric variance) may be defined as

$$\sigma^2 = \left\langle \|\hat{\boldsymbol{\delta}}\|^2 \right\rangle = \int_{\mathcal{D}} \int_{\mathcal{G}} \hat{\boldsymbol{\delta}}(\boldsymbol{\xi}, \mathbf{x}) \cdot \hat{\boldsymbol{\delta}}(\boldsymbol{\xi}, \mathbf{x}) p(\mathbf{x}) \mathrm{d}\boldsymbol{\xi} \mathrm{d}\mathbf{x} \tag{4}$$

where $\hat{\boldsymbol{\delta}} = \boldsymbol{\delta} - \langle \boldsymbol{\delta} \rangle$ and $\langle \cdot \rangle$ denotes the ensemble average over $\mathbf{x} \in \mathcal{D}$.

In this context, the aim of the KLE is to find an optimal basis of orthonormal functions, for the linear representation of $\hat{\boldsymbol{\delta}}$, expressed by

$$\hat{\boldsymbol{\delta}}(\boldsymbol{\xi}) \approx \sum_{k=1}^{N} \alpha_k \boldsymbol{\phi}_k(\boldsymbol{\xi}) \tag{5}$$

where α_k are the basis-function components, used hereafter as new design variables, and $\{\boldsymbol{\phi}_k\}_{k=1}^{\infty}$ (called KL modes) are the solutions of the eigenproblem

$$\mathcal{L}\boldsymbol{\phi}(\boldsymbol{\xi}) = \int_{\mathcal{G}} \left\langle \hat{\boldsymbol{\delta}}(\boldsymbol{\xi}, \mathbf{x}) \otimes \hat{\boldsymbol{\delta}}(\boldsymbol{\xi}', \mathbf{x}) \right\rangle \boldsymbol{\phi}(\boldsymbol{\xi}') \mathrm{d}\boldsymbol{\xi}' = \lambda \boldsymbol{\phi}(\boldsymbol{\xi}) \tag{6}$$

The reduced dimension N is selected in order to retain a prescribed level l (with $0 \leq l \leq 1$) of the original geometric variance. Using the property of the KLE eigenvalues (also called KL values), N in Eq. 5 is selected such as

$$\sum_{k=1}^{N} \lambda_k \geq l \sum_{k=1}^{\infty} \lambda_k = l\sigma^2 \tag{7}$$

with $\lambda_k \geq \lambda_{k+1}$. Details of equations and numerical implementations are given in [2].

2.4 Adaptive multi-fidelity metamodel

If one considers M functions of interest (relevant outputs), the multi-fidelity metamodel (MFM) is defined as

$$\begin{aligned} \hat{f}_i(\mathbf{x}) &= \tilde{f}_{i,L}(\mathbf{x}) + \tilde{\varepsilon}_i(\mathbf{x}), \qquad \text{with} \quad i = 1, \ldots, M \\ \varepsilon_i(\mathbf{x}) &= f_{i,H}(\mathbf{x}) - f_{i,L}(\mathbf{x}), \quad \text{with} \quad i = 1, \ldots, M \end{aligned} \tag{8}$$

where superscript "$\sim$" denotes the metamodel prediction, and ε_i is the difference (error) between high- and low-fidelity simulations ($f_{i,H}$ and $f_{i,L}$, respectively).

The uncertainty associated with the prediction provided by the MFM of the i-th function is defined as $U_{\hat{f}_i}(\mathbf{x}) = \sqrt{U^2_{\tilde{f}_{i,L}}(\mathbf{x}) + U^2_{\tilde{\varepsilon}_i}(\mathbf{x})}$, where $U_{\tilde{f}_{i,L}}$ and $U_{\tilde{\varepsilon}_i}$ are the uncertainties associated to the prediction of the i-th function, provided by the low-fidelity and error metamodels ($\tilde{f}_{i,L}$ and $\tilde{\varepsilon}_i$), respectively [10].

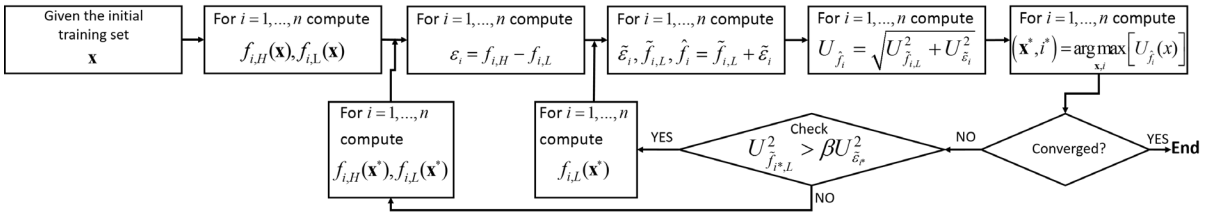

Figure 2: Multi-fidelity metamodel, adaptive sampling procedure

The MFM is trained using the adaptive procedure shown in Fig. 2, resulting in an adaptive MFM (AMFM). After initialization, a new sample is added to the training set at each iteration, solving $(\mathbf{x}^*, i^*) = \underset{\mathbf{x},i}{\operatorname{argmax}}[U_{\hat{f}_i}(\mathbf{x})]$. Once $\mathbf{x}^*$ and i^* are evaluated, the training sets H and/or L (high- and low-fidelity, respectively) are updated as

$$\begin{cases} \text{If } U^2_{\tilde{f}_{i^*,L}}(\mathbf{x}^*) \geq \beta U^2_{\tilde{\epsilon}_{i^*}}(\mathbf{x}^*), \text{ then add } \mathbf{x}^* \text{ to } L \\ \text{If } U^2_{\tilde{f}_{i^*,L}}(\mathbf{x}^*) < \beta U^2_{\tilde{\epsilon}_{i^*}}(\mathbf{x}^*), \text{ then add } \mathbf{x}^* \text{ to } H \text{ and } L \end{cases} \tag{9}$$

where $\beta \in [0, 1]$ is an arbitrary tuning parameter, related to the ratio of the computational cost of low- and high-fidelity simulations.

In the present work, the prediction $\tilde{f}$ is evaluated as the expected value (EV) of a set of stochastic RBF predictions [4], which depend on the stochastic parameter $\tau \sim \text{unif}[1, 3]$:

$$\tilde{f}(\mathbf{x}) = EV[g(\mathbf{x}, \tau)] \quad \text{with} \quad g(\mathbf{x}, \tau) = \sum_{j=1}^{J} w_j \, ||(\mathbf{x} - \mathbf{x}_j)||^{\tau} \tag{10}$$

where J is the size of the training set, $\mathbf{x}_j$ are the training points, and $\|\cdot\|$ is the Euclidean norm. The coefficients w_j are obtained by the linear system $\mathbf{A}\mathbf{w} = \mathbf{y}$ with $\mathbf{w} = \{w_j\}$. The elements of the matrix $\mathbf{A}$ are $a_{jk} = ||\mathbf{x}_j - \mathbf{x}_k||^{\tau}$ and the vector $\mathbf{y} = \{y_j\}$ collects the function evaluations at the training points, $y_j = f(\mathbf{x}_j)$.

The uncertainty $U(\mathbf{x})$ associated to the metamodel prediction is quantified at each $\mathbf{x}$ as the 95%-confidence interval of $g(\mathbf{x}, \tau)$. This is evaluated using a Monte Carlo sampling over τ, as shown in [4].

2.5 Potential flow solver WARP

The WAve Resistance Program (WARP) code, developed by the CNR-INSEAN [16], is used for the numerical solution of the potential flow equations. For the current application, wave resistance computations are based on the linear potential flow theory, with Dawson (or double-model) linearization. The wave resistance is evaluated using a pressure integral over the body surface, whereas the frictional resistance is estimated using a flat-plate approximation based on the local Reynolds number. Sinkage and trim are fixed (even keel).

The computational grids are defined using a refinement ratio of $\sqrt{2}$. The high- and low-fidelity grids (G1 and G2, respectively) have 5.2k and 2.6k panels for the body and 6k and 3k panels for the free-surface, respectively. Half domain is modelled, using problem symmetry. The computational domain dimensions are $1.5L_{\text{OA}}$ upstream, $3.5L_{\text{OA}}$ downstream, and $1.5L_{\text{OA}}$ sideways. Figure 3 shows the computational grids for the free surface and hull for both G1 (Fig. 3a,b) and G2 (Fig. 3c,d). For the current problem, each high-fidelity simulation requires an average wall-clock time of 4 minutes on an Intel Xeon E5-1620 v2 @3.70GHz, whereas each low-fidelity simulation requires 1 minute. The resulting computational-time ratio is $\beta = 0.25$.

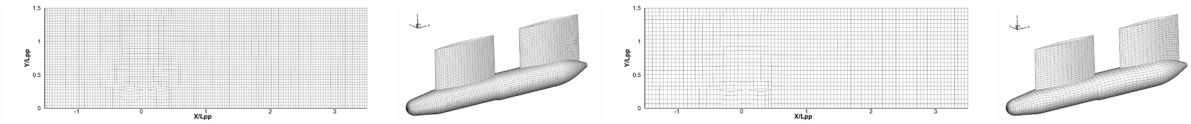

(a) G1, free surface (b) G1, body (c) G2, free surface (d) G2, body

Figure 3: High- and low-fidelity computational grids

2.6 Multi-objective deterministic PSO

PSO algorithm [11] is based on the social-behaviour metaphor of a flock of birds or a swarm of bees searching for food and belongs to the class of metaheuristic algorithms for single-objective

derivative-free global optimization. Pinto et al. [15] proposed a multi-objective deterministic version of PSO (MODPSO) as

$$\begin{cases} \mathbf{v}_i^{k+1} = \chi \left[\mathbf{v}_i^k + c_1 \left(\mathbf{p}_i - \mathbf{x}_i^k \right) + c_2 \left(\mathbf{g}_i - \mathbf{x}_i^k \right) \right] \\ \mathbf{x}_i^{k+1} = \mathbf{x}_i^k + \mathbf{v}_i^{k+1} \end{cases} \tag{11}$$

where $\mathbf{v}_i^k$ and $\mathbf{x}_i^k$ are the velocity and the position of the i-th particle at the k-th iteration, χ is a constriction factor, c_1 and c_2 are the cognitive and social learning rate, and $\mathbf{p}_i$ and $\mathbf{g}_i$ are the cognitive and social attractor.

The algorithm formulation and setup is defined as suggested in [17]: the cognitive attractor $\mathbf{p}_i$ is the personal minimizer of the aggregate function $F(\mathbf{x}_i) = \sum_{m=1}^{M} w_m f_m(\mathbf{x}_i)$, where $w_m = 1/M$ $(\forall m)$ is the weight associated to the m-th objective function with M the number of objective functions; the social attractor $\mathbf{g}_i$ is the closest point to the i-th particle of the Pareto front; the number of particles is set equal to 64 ($8MN_{\text{dv}}$), initialized over domain and boundary with a Hammersley distribution and non-null velocity [21]; the coefficients correspond to $\chi = 0.721$, $c_1 = c_2 = 1.655$ [22]; a semi-elastic wall-type approach [14] is used to keep the particles inside the feasible domain. The budget of problem evaluations is set equal to 16,000 ($2000MN_{\text{dv}}$).

3 NUMERICAL RESULTS

A preliminary assessment of the computational grids (G1 and G2) is performed. Figure 4 shows the total resistance evaluated using G1 and G2, along with the error $\varepsilon = R_T|_{G1} - R_T|_{G2}$ versus the advancing speed.

A number of $S = 11,500$ random designs are produced assuming a uniform distribution $p(\mathbf{x})$. Figure 5 shows the KLE results in terms of design variability associated to a reduced-dimensionality space of dimension N for $S = 3,000$, 6,000, and 11,500 samples. The results are found convergent versus S. The number of design variables is reduced to $N = 4$, retaining the 95% of the original variability. The corresponding KL modes are shown in Fig. 6. For the reduced-dimensionality representation of Eq. 5, modes are normalized such as $(\boldsymbol{\phi}_k, \boldsymbol{\phi}_k) = 3\lambda_k$, $\forall k$, assuming a uniform distribution for α_k. Accordingly, the new design variable range is set to $-1 < \alpha_k < 1$, $\forall k$. A preliminary sensitivity analysis is performed along the KL modes for R_T (Fig. 7a) and ∇ (Fig. 7b), respectively. It is worth noting that both R_T and ∇ are mainly influenced by the first two KL modes.

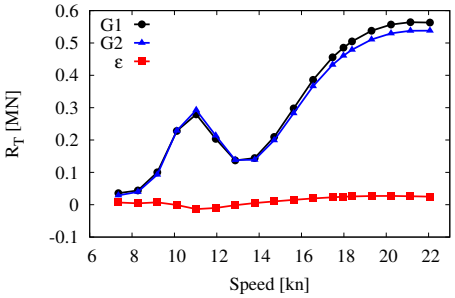

Figure 4: Total resistance versus speed

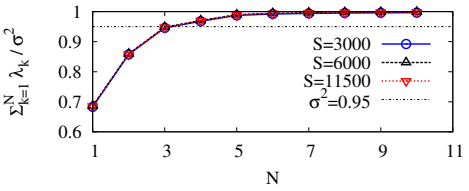

Figure 5: Normalized variance resolved by a reduced-dimensionality space of dimension N (KL values cumulative sum)

Sensitivity analysis values are used as initial training set for the AMFM, resulting in 17 high- and low-fidelity analysis. A convergence value for the maximum prediction uncertainty (U_{Max}) of the AMFM is set equal to 5% of the initial R_T and ∇ values. A maximum budget of 100 iterations is used for the adaptive sampling procedure. Unfeasible configurations are penalized.

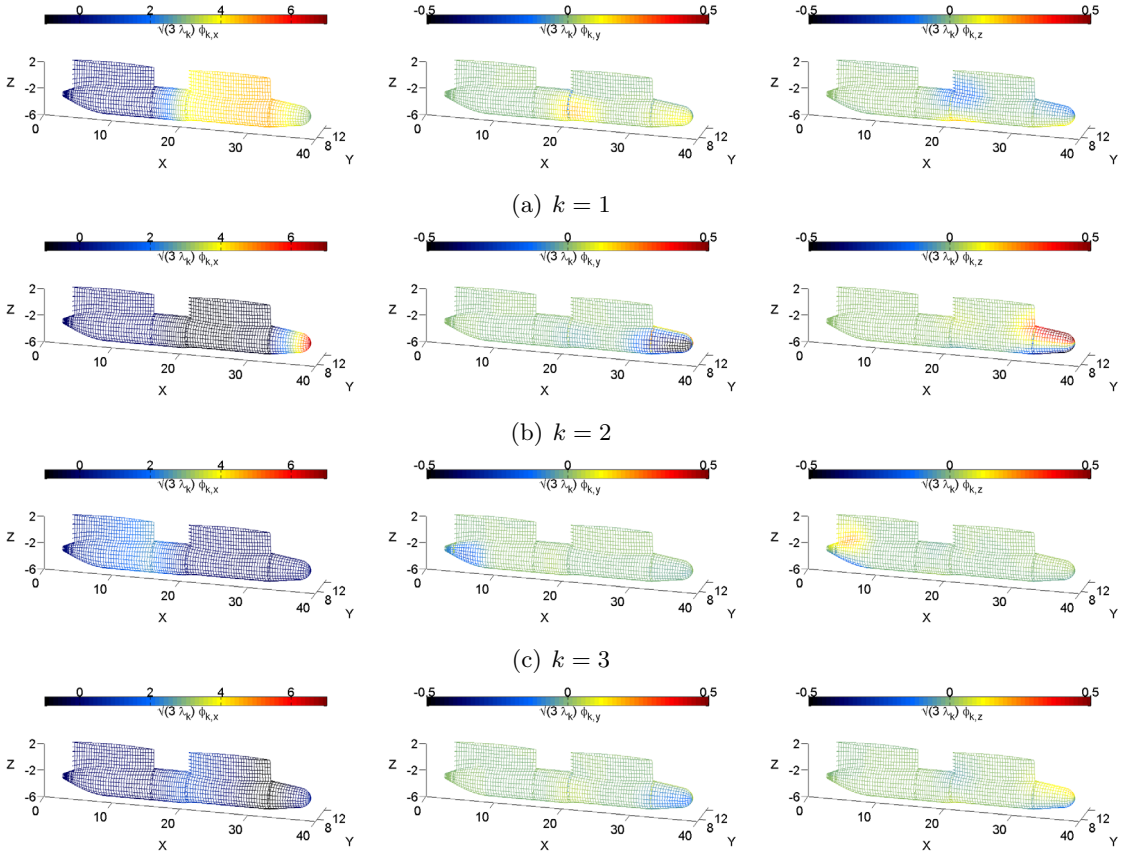

(a) $k = 1$

(b) $k = 2$

(c) $k = 3$

(d) $k = 4$

Figure 6: KL modes ($k = 1, \ldots, 4$), represented on the original (unmodified) grid

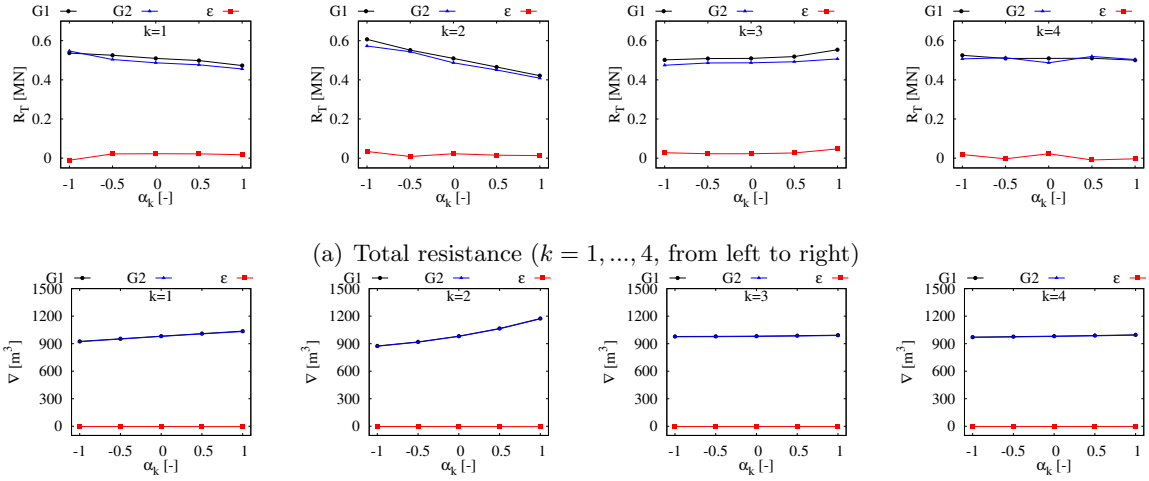

(a) Total resistance ($k = 1, ..., 4$, from left to right)

(b) Displacement ($k = 1, ..., 4$, from left to right)

Figure 7: Sensitivity analysis along KL modes

Figure 8 shows the convergence of U_{Max} for the prediction of R_T and ∇ during the adaptive training process. Square marks indicate where high-fidelity evaluations are performed, whereas arrows indicate where the penalization is used. The displacement maximum uncertainty decreases more rapidly and with less oscillations than that for the total resistance. The whole budget (100 iterations) is used for training the AMFM, achieving a U_{Max} is equal to 9.1% and 5.6% for R_T and ∇, respectively. A total of 117 low-fidelity and 27 high-fidelity evaluations are performed, including the initial training set, resulting in a total wall-clock time equal to 225 minutes on an Intel Xeon E5-1620 v2 @3.70GHz.

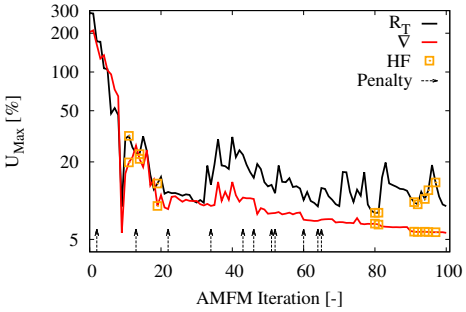

Figure 8: Prediction uncertainty through the adaptive sampling process

Figure 9a shows the Pareto front provided by the AMFM based MODPSO and three selected optimal designs: (A) maximum total resistance reduction, (B) maximum displacement increase, and (C) minimum aggregate objective function (with equal weights). The corresponding optimal design variables values are shown in Fig. 9b. Figure 9c shows the total resistance versus the speed for the original and the three optimal designs. All the selected designs perform better than the original SWATH at 18 kn, whereas the original design shows better performances at lower and higher speeds. Table 1 summarizes the main geometric changes (L_{OA}, S_{W}, and A_{WP}) associated to the optimized configurations along with AMFM predictions and actual fine-grid evaluations by WARP.

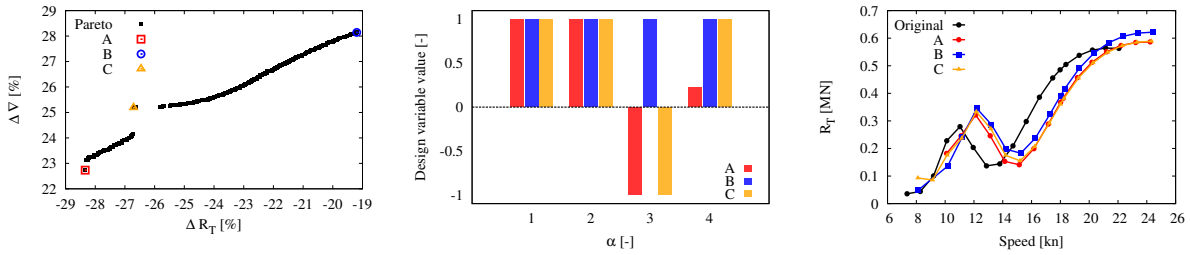

(a) Pareto front and optimal designs (b) Optimal design variables (c) Total resistance versus speed

Figure 9: Optimization results and comparison between original and selected optimal designs performance

Table 1: Optimal designs geometry and performance, comparison of AMFM predictions to WARP

				ΔR_T%		$\Delta\nabla$%	
Design	ΔL_{OA}%	ΔS_{W}%	ΔA_{WP}%	AMFM	WARP	AMFM	WARP
A	20.55	19.60	-5.65	-28.3	-24.3	22.7	22.8
B	22.19	24.33	1.27	-19.2	-19.2	28.1	28.2
C	21.64	20.10	-11.42	-26.7	-25.7	25.2	25.1

Finally, Fig. 10a compares the wave elevation of optimal (C) and original designs. The optimized configuration produces a diverging Kelvin wave that is significantly reduced. Figure 10b shows the pressure distribution on the optimal (C) and original hulls. The optimized hull shows lower pressure gradients and a better pressure recovery towards the stern. Figure 10c

shows comparison between the optimized and original hulls. The optimized SWATH is more than 20% longer ($L_{\mathrm{OA}} = 44.4$ m) than the original, whereas the strut length is about 8.4% smaller ($S_{\mathrm{L}} = 11.0$ m).

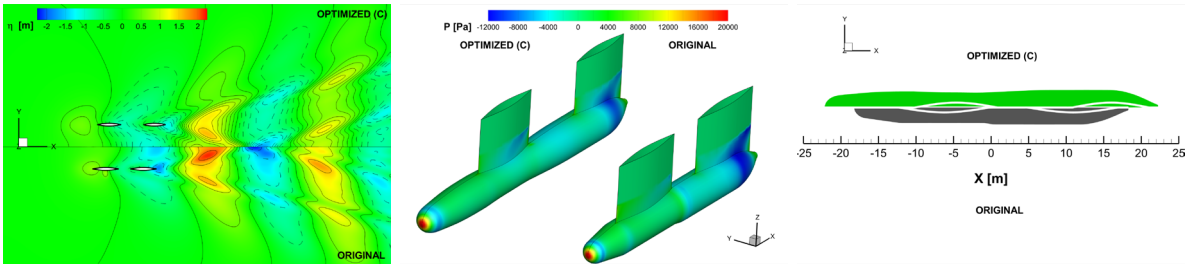

(a) Wave elevation (b) Pressure (c) Geometry top view

Figure 10: Detailed comparison of optimized (C) and original designs

4 CONCLUSIONS

A multi-objective SBDO of a 36.5 m SWATH has been assessed for the reduction of the total resistance at 18 kn and the increase of the displacement.

The geometry has been realized as a parametric model within CAESES® using 27 design parameters. The Sobol engine available in CAESES® has been used to modify the original geometry and provide data to the design-space dimensionality reduction method by KLE. The original design space has been reduced in dimensionality to 4 variables, while resolving more than the 95% of the original geometric variability associated to the shape modification. The KL modes have been used as a basis to built the new reduced-dimensionality design space.

An adaptive multi-fidelity metamodel has been trained by the potential flow solver WARP using two grids, namely defining the high- and low-fidelity evaluations. The adaptive sampling procedure has required the whole budget of 100 iterations, achieving a prediction uncertainty equal to 9.1% and 5.6% for total resistance and displacement, respectively. Specifically, 27 high- and 117 low-fidelity evaluations have been used. A comparison of metamodel predictions and high-fidelity evaluations has been carried out for selected designs, showing a close agreement.

The optimization has been carried out on the metamodel using a MODPSO algorithm, obtaining a discontinuous and convex/concave Pareto front. The topology of the front is likely due to the metamodel, which may not have achieved full training convergence. Optimization achievements have been found significant for both R_T ($-19 \div 18\%$) and ∇ ($+23 \div 28\%$). Three optimal designs have been identified for (A) maximum total resistance reduction, (B) maximum displacement increase, and (C) minimum aggregate objective (with equal weights).

These designs perform better than the original at 18 kn, whereas the original design shows better performances in lower and higher speed ranges. This difference is mainly due to a significant change in length of the optimized designs, which reflects in a reduced Froude number at 18 kn. This motivates further investigations via robust design optimization for a stochastic speed ranges. Wave elevation and pressure distribution has been shown for design C, emphasizing the beneficial effects of the shape optimization.

The optimized designs finally show a significant increase of the wet surface (+20% or more) and variation of the water-plane area (from –11 to +1%). This motivates future extensions to Reynolds-averaged Navier-Stokes solvers (to address viscous effects), along with the proper

inclusion in the optimization of critical design constraints associated to the intact pitch and roll stability, seakeeping, and structural analysis, not considered at the current stage of the work.

ACKNOWLEDGEMENTS

Developments of the SBDO methodologies has been partially supported by the Office of Naval Research, NICOP grant N62909-15-1-2016, administered by Dr. Woei-Min Lin and, and by the Italian Flagship Project RITMARE, founded by the Italian Ministry of Education.

REFERENCES

[1] Harries, S., Abt, C. and Brenner, M. Upfront CAD–parametric modeling techniques for shape optimization, *EUROGEN 2015, International Conference on Evolutionary and Deterministic Methods for Design, Optimization and Control with Applications to Industrial and Societal Problems*, Glasgow, UK, September, (2015).

[2] Diez, M., Campana, E. F. and Stern, F. Design-space dimensionality reduction in shape optimization by Karhunen–Loève expansion, *Computer Methods in Applied Mechanics and Engineering*, **283**, 1525–1544, (2015).

[3] Simpson, T. W., Poplinski, J., Koch, P. N. and Allen, J. K. Metamodels for computer-based engineering design: survey and recommendations, *Engineering with Computers*, **17** (2), 129–150, (2001).

[4] Volpi, S., Diez, M., Gaul, N., Song, H., Iemma, U., Choi, K. K., Campana, E. F. and Stern, F. Development and validation of a dynamic metamodel based on stochastic radial basis functions and uncertainty quantification, *Structural and Multidisciplinary Optimization*, **51** (2), 347–368, (2015).

[5] Diez, M., Volpi, S., Serani, A., Stern, F. and Campana, E. F. Simulation-based design optimization by sequential multi-criterion adaptive sampling and dynamic radial basis functions, *EUROGEN 2015, International Conference on Evolutionary and Deterministic Methods for Design, Optimization and Control with Applications to Industrial and Societal Problems*, Glasgow, UK, September, (2015).

[6] Haftka, R. T., Villanueva, D. and Chaudhuri, A. Parallel surrogate-assisted global optimization with expensive functions – a survey, *Structural and Multidisciplinary Optimization*, pp. 1–11, (2016).

[7] Alexandrov, N., Nielsen, E., Lewis, R. and Anderson, W. First-order model management with variable-fidelity physics applied to multi-element airfoil optimization, *AIAA paper*, **4886**, (2000).

[8] Sun, G., Li, G., Stone, M. and Li, Q. A two-stage multi-fidelity optimization procedure for honeycomb-type cellular materials, *Computational Materials Science*, **49** (3), 500–511, (2010).

[9] de Baar, J., Roberts, S., Dwight, R. and Mallol, B. Uncertainty quantification for a sailing yacht hull, using multi-fidelity kriging, *Computers & Fluids*, **123**, 185–201, (2015).

[10] Pellegrini, R., Leotardi, C., Iemma, U., Campana, E. F. and Diez, M. Multi-fidelity adaptive global metamodel of expensive computer simulations, *Proceedings of the IEEE World Congress on Computational Intelligence, IEEE WCCI 2016*, Vancouver, Canada, 24–29 July, (2016).

[11] Kennedy, J. and Eberhart, R. Particle swarm optimization, *Proceedings of the IEEE International Conference on Neural Networks*, Vol. 4, pp. 1942–1948, (1995).

[12] Moore, J. and Chapman, R. Application of particle swarm to multiobjective optimization, *Department of Computer Science and Software Engineering, Auburn University*, (1999).

[13] Lalwani, S., Singhal, S., Kumar, R. and Gupta, N. A comprehensive survey: Applications of multi-objective particle swarm optimization (MOPSO) algorithm, *Transactions on Combinatorics*, **2** (1), 39–101, (2013).

[14] Serani, A., Leotardi, C., Iemma, U., Campana, E. F., Fasano, G. and Diez, M. Parameter selection in synchronous and asynchronous deterministic particle swarm optimization for ship hydrodynamics problems, *Applied Soft Computing*, **49**, 313 – 334, (2016).

[15] Pinto, A., Peri, D. and Campana, E. F. Multiobjective optimization of a containership using deterministic particle swarm optimization, *Journal of Ship Research*, **51** (3), 217–228, (2007).

[16] Bassanini, P., Bulgarelli, U., Campana, E. F. and Lalli, F. The wave resistance problem in a boundary integral formulation, *Surveys on Mathematics for Industry*, **4**, 151–194, (1994).

[17] Pellegrini, R., Campana, E. F., Diez, M., Serani, A., Rinaldi, F., Fasano, G., Iemma, U., Liuzzi, G., Lucidi, S. and Stern, F. Application of derivative-free multi-objective algorithms to reliability-based robust design optimization of a high-speed catamaran in real ocean environment, *Engineering Optimization IV - Rodrigues et al. (Eds.)*, (2014).

[18] Sobol', I. M. On the distribution of points in a cube and the approximate evaluation of integrals, *U.S.S.R Computational Mathematics and Mathematical Physics*, **7** (4), 86–112, (1967).

[19] Iemma, U., Morino, L. and Diez, M. Digital holography and Karhunen-Loève decomposition for the modal analysis of two-dimensional vibrating structures, *Journal of Sound and Vibration*, **291** (1), 107–131, (2006).

[20] Iemma, U., Diez, M. and Morino, L. An extended Karhunen-Loève decomposition for modal identification of inhomogeneous structures, *Journal of Vibration and Acoustics*, **128**, 357, (2006).

[21] Chen, X., Diez, M., Kandasamy, M., Zhang, Z., Campana, E. F. and Stern, F. High-fidelity global optimization of shape design by dimensionality reduction, metamodels and deterministic particle swarm, *Engineering Optimization*, **47** (4), 473–494, (2015).

[22] Clerc, M. Stagnation analysis in particle swarm optimization or what happens when nothing happens, *Online at http://clerc. maurice. free. fr/pso*, (2006).